UILU-ENG-95-2007

CIVIL ENGINEERING STUDIES

STRUCTURAL RESEARCH SERIES NO. 603

ISSN: 0069-4274

Constraint Effects on Fracture Toughness of Impact Loaded, Pre-cracked Charpy Specimens

By
KYLE C. KOPPENHOEFER
and
ROBERT H. DODDS, JR.

A Report on a Research Project
Sponsored by the
U.S. NUCLEAR REGULATORY COMMISSION
OFFICE OF NUCLEAR REGULATORY RESEARCH
DIVISION OF ENGINEERING
WASHINGTON, D.C.

DEPARTMENT OF CIVIL ENGINEERING
UNIVERSITY OF ILLINOIS AT
URBANA-CHAMPAIGN
URBANA, ILLINOIS
JUNE 1995

50272–101

REPORT DOCUMENTATION PAGE	1. REPORT NO. UILU–ENG–95–2007	2.	3. Recipient's Accession No.

4. Title and Subtitle
Constraint Effects on Fracture Toughness of Impact Loaded, Pre-cracked Charpy Specimens

5. Report Date
June 1995

6.

7. Author(s)
Kyle C. Koppenhoefer and R.H. Dodds, Jr.

8. Performing Organization Report No.
SRS 603

9. Performing Organization Name and Address
University of Illinois at Urbana–Champaign
Department of Civil Engineering
205 N. Mathews Avenue
Urbana, Illinois 61801

10. Project/Task/Work Unit No.

11. Contract(C) or Grant(G) No.
N00167–92–K–0038

12. Sponsoring Organization Name and Address
U.S. Nuclear Regulatory Commission
Office of Nuclear Regulatory Research
Division of Engineering
Washington, DC 20555

13. Type of Report & Period Covered
1–1–95 to 6–30–95

14.

15. Supplementary Notes

16. Abstract (Limit: 200 words)

Impact loaded, pre-cracked Charpy specimens often play a crucial role in irradiation surveillance programs for nuclear power plants. However, the small specimen size ($B = W = 10$ mm) limits the maximum value of cleavage fracture toughness (J_c) that can be measured under elastic-plastic conditions without loss of crack tip constraint. In this investigation, plane-strain impact analyses provide detailed resolution of crack–tip fields for impact loaded specimens. Crack–tip stress fields are characterized in terms of J–Q trajectories and the Toughness Scaling Model which is applicable for a cleavage fracture mechanism. Results of the analyses suggest deformation limits at fracture in the form of $b > MJ_c/\sigma_0$, where M approaches 25–30 for a strongly rate sensitive material at impact velocities of 3–6 m/s. Based on direct comparison of the static and dynamic J–values computed using a domain-integral formulation, a new proposal emerges for the transition time, the time after impact at which inertial effects diminish sufficiently for simple evaluation of J using the plastic eta factor approach.

17. Document Analysis a. Descriptors

Inelastic Fracture, Charpy Specimen, Finite Elements, J–Integrals, Impact Testing, Size Effects

b. Identifiers/Open–Ended Terms

c. COSATI Field/Group

18. Availability Statement
Release Unlimited

19. Security Class (This Report)
UNCLASSIFIED

21. No. of Pages
21

20. Security Class (This Page)
UNCLASSIFIED

22. Price

(See ANSI–Z39.18)

OPTIONAL FORM 272 (4–77)
Department of Commerce

Constraint Effects on Fracture Toughness of Impact Loaded, Pre-cracked Charpy Specimens

By

Kyle C. Koppenhoefer

Department of Civil Engineering
University of Illinois

Robert H. Dodds, Jr.

Department of Civil Engineering
University of Illinois

A Report on a Research Project Sponsored by the:

U.S. NUCLEAR REGULATORY COMMISSION
OFFICE OF NUCLEAR REGULATORY RESEARCH
DIVISION OF ENGINEERING

WASHINGTON, DC 20555

University of Illinois
Urbana, Illinois
June 1995

ABSTRACT

Impact loaded, pre-cracked Charpy specimens often play a crucial role in irradiation surveillance programs for nuclear power plants. However, the small specimen size ($B = W = 10$ mm) limits the maximum value of cleavage fracture toughness (J_c) that can be measured under elastic-plastic conditions without loss of crack tip constraint. In this investigation, plane-strain impact analyses provide detailed resolution of crack–tip fields for impact loaded specimens. Crack–tip stress fields are characterized in terms of J–Q trajectories and the Toughness Scaling Model which is applicable for a cleavage fracture mechanism. Results of the analyses suggest deformation limits at fracture in the form of $b > MJ_c/\sigma_0$, where M approaches 25–30 for a strongly rate sensitive material at impact velocities of 3–6 m/s. Based on direct comparison of the static and dynamic J–values computed using a domain-integral formulation, a new proposal emerges for the transition time, the time after impact at which inertial effects diminish sufficiently for simple evaluation of J using the plastic eta factor approach.

ACKNOWLEDGEMENTS

This investigation was supported by grants principally from the U.S. Nuclear Regulatory Commission and the Naval Surface Warfare Center–Annapolis Detachment (Code 614). The authors express their appreciation to colleagues Drs. Kim Wallin (VTT Finland) and Richard Link (NSWC).

1. Introduction

Conventional nonlinear fracture mechanics often characterizes material toughness for static loading using the parameters J_c (for brittle fracture), J_{Ic} (for the onset of stable tearing) and J_R–Δa (for tearing resistance). Laboratory tests to measure these parameters use standard geometries with fatigue sharpened cracks, for example a single edge notch bend specimen, loaded to fracture under nominally static conditions. Specimens typically have a minimum size of width (W) = 50 mm, thickness (B) = 25 mm, span (S) = 200 mm (= 4W) with a crack depth (a) such that $a/W \geq 0.5$. Larger specimens, which maintain the same geometric proportions, may be required to satisfy limits on the amount of plastic deformation at fracture to insure a valid description of the material toughness using a single parameter description (J)[1,17]. The test procedures record applied load, load–line displacement and crack mouth opening displacement (CMOD) for use in computing applied J–values. The static loading and relatively deep notches enable application of straightforward data acquisition techniques to measure these quantities.

As often happens in engineering applications, the amount of material needed to conduct a "standard" fracture test described above may not be available. Examples of these situations include: material extracted from surveillance capsules of nuclear pressure vessels, small samples of experimental alloys under development and trepan samples taken from structures currently in service. In still other instances, sufficient material may be available but the cost to perform the test may be prohibitive—this situation calls for a rapid, low–cost "screening" test.

The need to characterize fracture toughness using small amounts of material, coupled with a low cost per test, often leads investigators to adopt the Charpy V–notch (CVN) specimen (ASTM E–23 [2]), with dimensions indicated in Figure 1. The specimen contains a blunt notch of root radius 0.25 mm which is *not* sharpened by fatigue cracking prior to the test. The specimen preparation and test procedure for the CVN is relatively simple; however, the data obtained from this test procedure limit the engineer to a *qualitative* comparison of impact toughness and ductility for a range of metals. Empirical correlations between fracture toughness (e.g. K_{Ic}) and Charpy impact energy (CVE), have been proposed by various researchers [5,24,13] to estimate *quantitatively* the fracture toughness for specific classes of metals. The standard CVN test procedure limits severely the applicability and extension of these empirical correlations due to the significant difference between the displacement, stress and strain fields ahead of a blunt notch and a fatigue sharpened crack tip. By conducting a series of conventional fracture toughness and CVN tests on 4340 steels subjected to various heat treatments, Ritchie [23] demonstrates an inverse relationship between fracture toughness and CVE (contrary to predictions of typical correlations) which he concludes is due to the stress and strain fields sampling different microstructurally relevant distances ahead of the notch/crack tip.

Experimental testing programs with limitations on available material volume but without the need for a low-cost procedure often use a modified Charpy V-notch test. Typical changes to the ASTM E–23 [2] procedure include sharpening the blunt notch via fatigue cracking and instrumentation to measure the dynamic load, load-line displacement and CMOD. Pre-

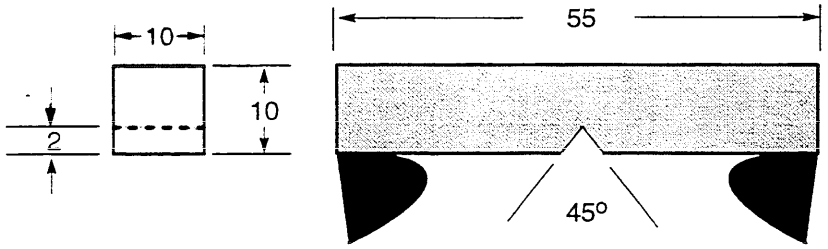

Figure 1. Charpy V-notch specimen (all length dimensions given in mm)

cracking the CVN eliminates previously stated concerns about blunt versus sharp notched specimens. Instrumentation increases greatly the experimental complexity (and cost) of each test, but it removes the need for determining fracture toughness through experimental correlations. The measurement of load, load-line displacement, and CMOD enables determination of the applied–J through the absorbed energy (plastic-eta factor) procedure typically used in static testing[]. However, a conversion of absorbed energy to J-values does not currently reflect potential effects of impact loading.

This paper describes results of computational studies of a *precracked* Charpy V-notch specimen ($a/W = 0.5$) subjected to impact loading. The finite element analyses provide two key results for engineering applications: (1) the time after impact at which inertial effects no longer affect the crack-tip fields; and (2) recommended limits on measured *cleavage* toughness values (denoted J_c) to maintain near-tip stresses at SSY levels expressed by $b > MJ_c/\sigma_0$ with b the remaining ligament, σ_0 the average of yield and ultimate stresses. The deformation/size limit derived from plane strain, static analyses (M=200) is overly strict for impact analyses of materials exhibiting even a moderate rate sensitivity; our plane strain analyses demonstrate that M varies strongly with the material strain-rate sensitivity. M-values as low as 25 are found for extremely rate sensitive materials.

2. Computational Procedures

Short duration impact loading of fracture specimens with sufficient mesh refinement to resolve the crack tip fields presents special challenges for finite element analyses. These include: the need to resolve both stress-wave effects upon impact and the response at much longer times near the fracture point, robust models to predict viscoplastic response of the material, extremely large numbers of degrees of freedom, and very large differences in relative element sizes over the models. These requirements led to use of the WARP3D [12] code.

WARP3D is a finite element code which computes the nonlinear dynamic response of three-dimensional solids under general loadings. The code solves the nodal equilibrium equations

$$\boldsymbol{I} + \boldsymbol{M}\ddot{\boldsymbol{u}} = \boldsymbol{P} \tag{1}$$

where $\boldsymbol{I}$ is the internal force vector, $\boldsymbol{M}$ is the structural mass matrix, $\ddot{\boldsymbol{u}}$ is the acceleration vector, and $\boldsymbol{P}$ is the load vector. Numerical time integration of the equations of motion in WARP3D is performed using the Newmark β-method [18].

Nonlinearity in $\boldsymbol{I}$ arises from the geometric and/or material effects while $\boldsymbol{P}$ becomes nonlinear when tractions applied to element faces have constant orientations relative to the deformed face. Solution of these nonlinear equations is achieved through Newton's method, an iterative procedure which drives residual nodal forces to zero. The residual force vector, $\boldsymbol{R}$, at any time is expressed as

$$\boldsymbol{R} = \boldsymbol{P} - \boldsymbol{I} - \boldsymbol{M}\ddot{\boldsymbol{u}} \ . \tag{2}$$

Newton's method for solving nonlinear equations follows by assuming there exists an approximate displacement state in the neighborhood of the exact solution for which a linear mapping provides a good approximation to the residual force vector. The essential equation driving the iterative solution in Newton's method becomes

$$\boldsymbol{K}_T^d \delta \boldsymbol{u}_{n+1}^i = \boldsymbol{P}_{n+1}^d - \boldsymbol{I}_{n+1}^{i-1} - \frac{1}{\beta \Delta t^2} \boldsymbol{M} \Delta \boldsymbol{u}_{n+1}^{i-1} \tag{3}$$

where $\boldsymbol{K}_T^d$ denotes the dynamic tangent stiffness matrix. The vector $\delta \boldsymbol{u}_{n+1}^i$ represents the corrective displacement increment for iteration i, $\boldsymbol{P}_{n+1}^d$ defines the dynamic load vector, β the

Newmark parameter ($\beta = 1/4$ in WARP3D), and Δt the time step. Subscripts denote the time step while the superscripts indicate the iteration.

Solution of the linear set of equations described by Eq. (3) is accomplished either by a direct solver or by a linear preconditioned conjugate gradient (LPCG) solver. The direct solver uses a highly optimized, version of Choleski factorization and back substitution based on multiple minimum degree ordering of the upper-triangular portion of the dynamic tangent stiffness matrix for the structure. The LPCG solver forms the basis for efficient solution of large 3-D models in WARP3D and uses an algorithm involving the iterative improvement of an approximate nodal displacement vector through a sequence of matrix operations.

The eight-node, isoparametric element provides the meshing capability in WARP3D. The element formulation employs a conventional tri-linear displacement field. With the $\overline{\mathbf{B}}$ modifications of Hughes [10], the element exhibits minimal locking under fully incompressible material response.

The small-strain plasticity model derives from rate independent J_2 flow theory with isotropic hardening. The rate independent (inviscid) stress-strain curve for uniaxial tension is described by a linear power-law model. A viscoplastic response is introduced through a power-law relationship suitable for ductile metals to describe the equivalent plastic strain rate:

$$\dot{\varepsilon}^{vp} = \frac{1}{\eta}\left[\left(\frac{q}{\sigma_e}\right)^m - 1\right] \tag{4}$$

where η and m are user-specified material constants, q denotes the rate-dependent (uniaxial) tensile stress and σ_e the inviscid (uniaxial) tensile stress. An example of the viscoplastic response predicted by this constitutive model appears in Figure 2. The material constant η elevates the non-linear part of the rate independent stress-strain curve without modifying the shape. The m-power changes the yield strength and strain hardening of the material model (both quantities increase with *decreasing* m-power).

3. Computational Models

3.1 Small-Scale Yielding Models

The solution for a single-ended crack in an infinite body provides the idealized reference state needed to quantify the effects of finite size on the crack-tip stress fields. The boundary layer model (Figure 3), originally proposed by Rice and Tracy [21] and McMeeking [14], consists of a circular region containing the edge crack. Displacements are applied to the outer circular edge of this region consistent with the linear elastic ($T = 0$) solution for a Mode I crack in an infinite body. Provided the plastic zone size (R_p) remains small relative to the size of the modeled region ($R_p \leq 0.05R$), self-similar solutions exist for the near-tip fields which scale with J/σ_0.

For evaluation of finite size effects under impact loading, the SSY model is subjected to remote loading rates ($\dot{K}_I$) comparable to those predicted for the precracked CVN specimen but with material inertia neglected. Analyses of both the SSY and CVN models use the same viscoplastic constitutive model.

3.2 Precracked CVN Models

The precrack CVN represents a modified three-point bend specimen having $a/W = 0.5$ with overall dimensions given in Figure 1. The specified displacement boundary conditions impose a loading history characteristic of a pendulum impacting on the specimen. The finite element

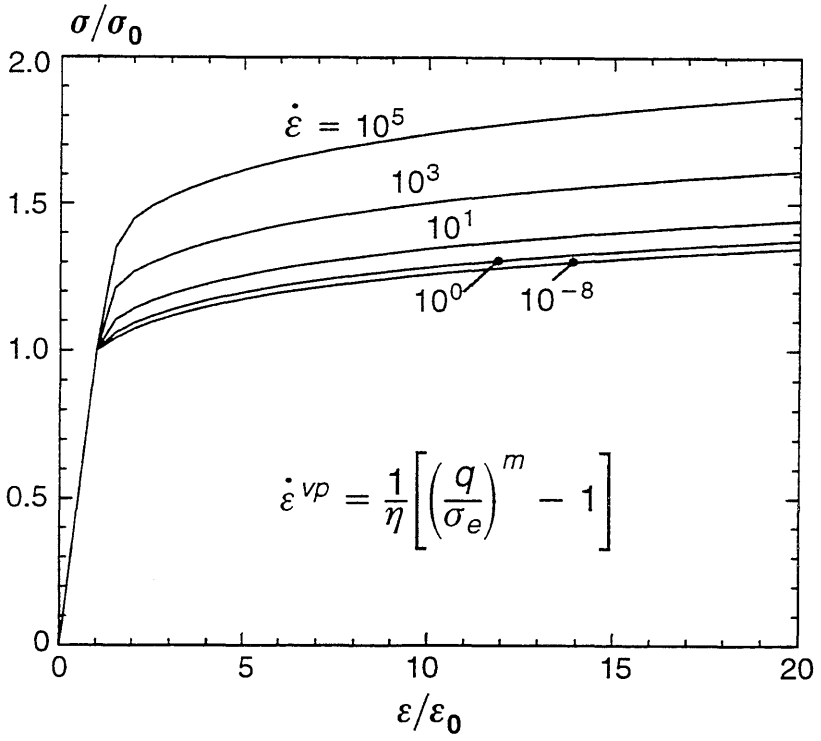

Figure 2. Normalized stress-strain curves over a range of strain rates for A533B pressure vessel steel at 100°C. The equation for the viscoplastic strain rate is also given. The values of η and m used to generate these curves are 1.0 $(1/sec)$ and 35, respectively.

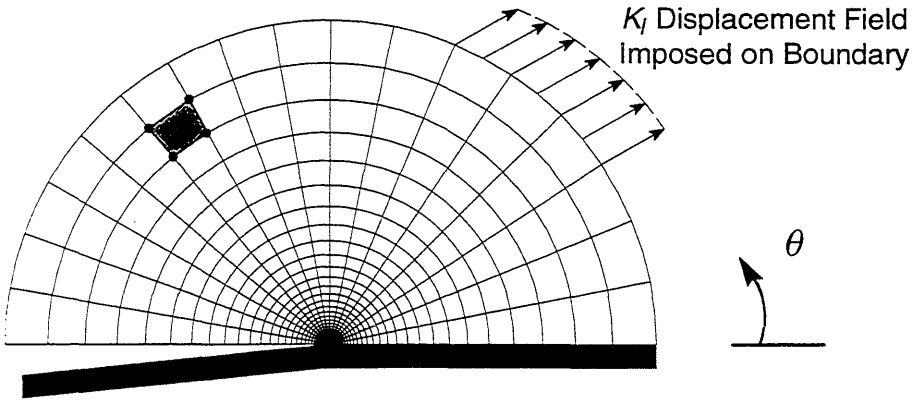

Figure 3. Small Scale Yielding (SSY) model.

mesh shown in Figure 4 defines a half-symmetric model constructed from eight-node, three-dimensional isoparametric elements. The model contains 2002 nodes in a single layer of 916 elements. The out-of-plane degrees-of-freedom (w) are constrained to enforce plane-strain conditions. The semi-circular mesh focuses on the crack tip to resolve the stress/strain fields over microstructurally relevant distances (2–10 × Crack Tip Opening Displacement). The crack-tip region contains 13 (total) elements in the θ direction with 10 elements defined over the region between 0° and 112.5° (θ = 0 on the crack plane ahead of the tip).

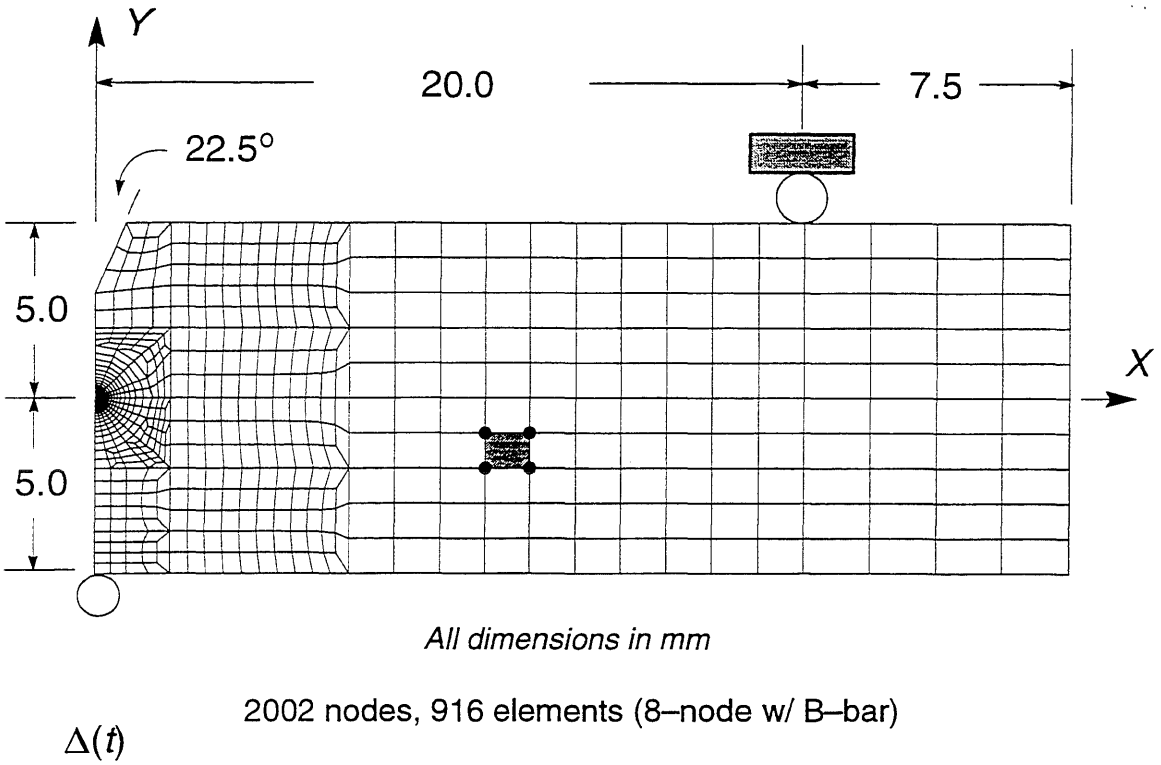

Figure 4. Finite element model of precracked CVN specimen.

The non-zero displacement boundary conditions, as shown in Figure 5, impose a constant velocity at the impact point. Over a short transitional time (0→4 μs) the velocity ramps from zero to the impact loading rate of the striker (this ramping reduces spurious oscillations in the response). Analyses are conducted for five impact rates (i.e. $v = 0.025, 0.25, 1.0, 3.0,$ and 6.0 m/s) to determine the effect of loading rate on specimen response. The 3.0 and 6.0 m/s impact rates match the lower and upper bound loading rates for standard CVN testing, as specified in ASTM E–23 [2].

Contributing factors for the specimen response are examined using three types of analyses: (1) static, (2) impact with inviscid material response, and (3) impact with viscoplastic material response. The viscoplastic analyses reflect a large range of material sensitivity to strain rate ($m = 35$; $\eta = 10^{-3}, 10^{-2}, 10^{-1}, 1, 10^{2}, 10^{3}, 10^{4}$).

4. Results and Discussion

4.1 Effects of Loading Scheme

Loading of the specimen through imposed displacements, as proposed by Ayers [4] and illustrated in Figure 5, simplifies considerably the numerical analysis of the CVN specimen. However, this scheme may not model realistically the impact load applied in Charpy testing. Rigorous numerical modelling of impact problems requires contact–separation finite elements, such as implemented in the ABAQUS/Explicit software package. Application of this code enables accurate modeling of the contact and separation conditions that exist between the specimen and the striker during a test. We conducted a plane-strain, contact–separation analysis of a coarsely meshed CVN specimen using ABAQUS/Explicit with the specimen impacted by a rig-

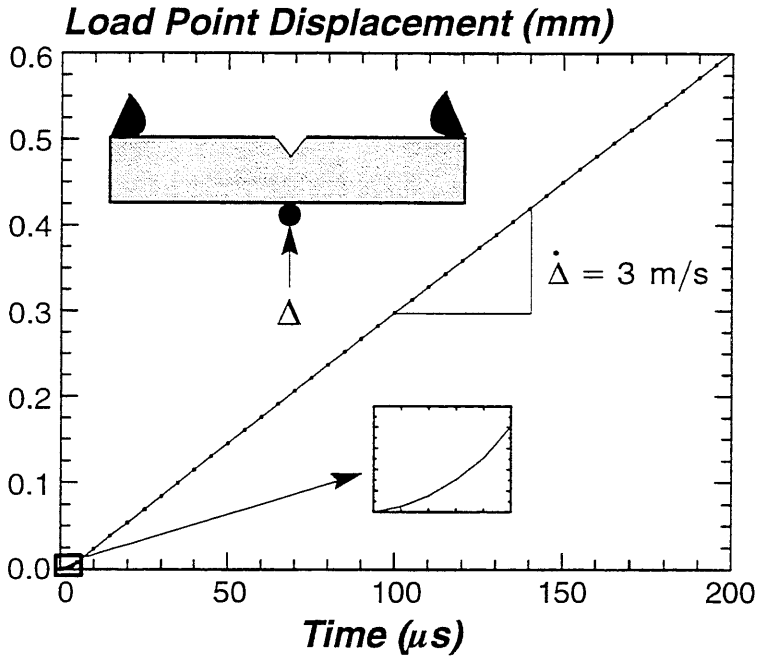

Figure 5. Total displacement applied to outer–edge, crackplane node of CVN model for the 3 m/s analysis. The final slope of this curve defines the impact loading rate.

id cylinder (8 mm radius) having a velocity of 3 m/s. Figure 6 compares the contact force from this analysis with the reaction force at the point of displacement application in the simplified loading scheme. The load predicted by the contact–separation model oscillates about the load predicted by the applied displacement model. Norris [19] and Ayers [4] demonstrated that such variations in the boundary forces do not carry over into the internal energy and J for the specimen, both of which increase monotonically with time. Our computations using the simplified scheme reveal similar responses as shown in Fig. 7. At present, we appeal to this feature of the impact response to justify loading the CVN models by the imposed displacements indicated in Figure 5.

4.2 Transition Times

The transition time, t_c, indicates the point after impact at which inertial effects on the crack-tip fields begin to diminish. Nakamura, Shih and Fruend [16] defined the transition time as the time at which the ratio of kinetic to deformation energy of a specimen decreases below unity. They calculated $t_c = 27W/c_1$ (=53 μs for a steel CVN, $a/W = 0.5$) for a three-point bend specimen subjected to a loading rate approximately one-half of the loading rate imposed on the CVN analyses described here.

The application of this energy measure, as shown in Figure 8, yields a transition time of $t_c = 14W/c_1$ (=28 μs for a steel CVN, $a/W = 0.5$) for the inviscid and viscoplastic analyses of the CVN specimen impacted at 3 m/s. Norris [19] reported kinetic and internal energies for a CVN specimen at an impact rate of 5.1 m/s, and these data provide a value of $t_c = 12W/c_1$. The significant difference between the transition times of the CVN specimen and those calculated by Nakamura, et al. [16] may be due in part to the difference in specimen configuration. Böhme and Kalthoff [7] determined experimentally that increasing the amount of material beyond the support point (i.e. extending the specimen length while holding the span fixed) dampens the oscillations in measured K_I values. The typical SE(B) specimen, as analyzed by Naka-

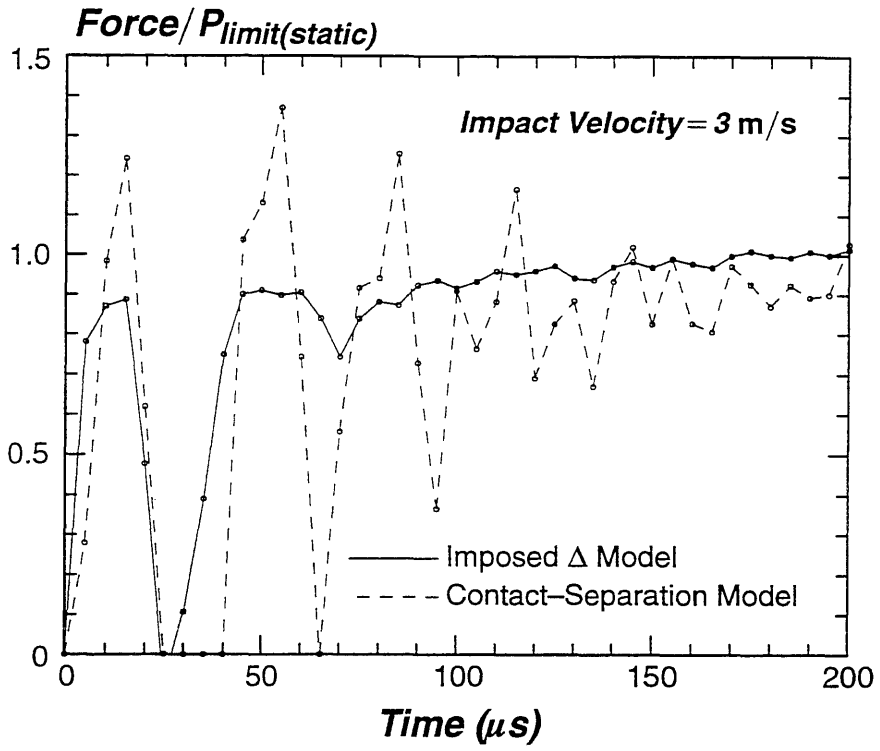

Figure 6. Normalized force versus time for contact analysis and displacement controlled analysis. $P_{limit\ (static)}$ is the computed static limit load for the CVN specimen.

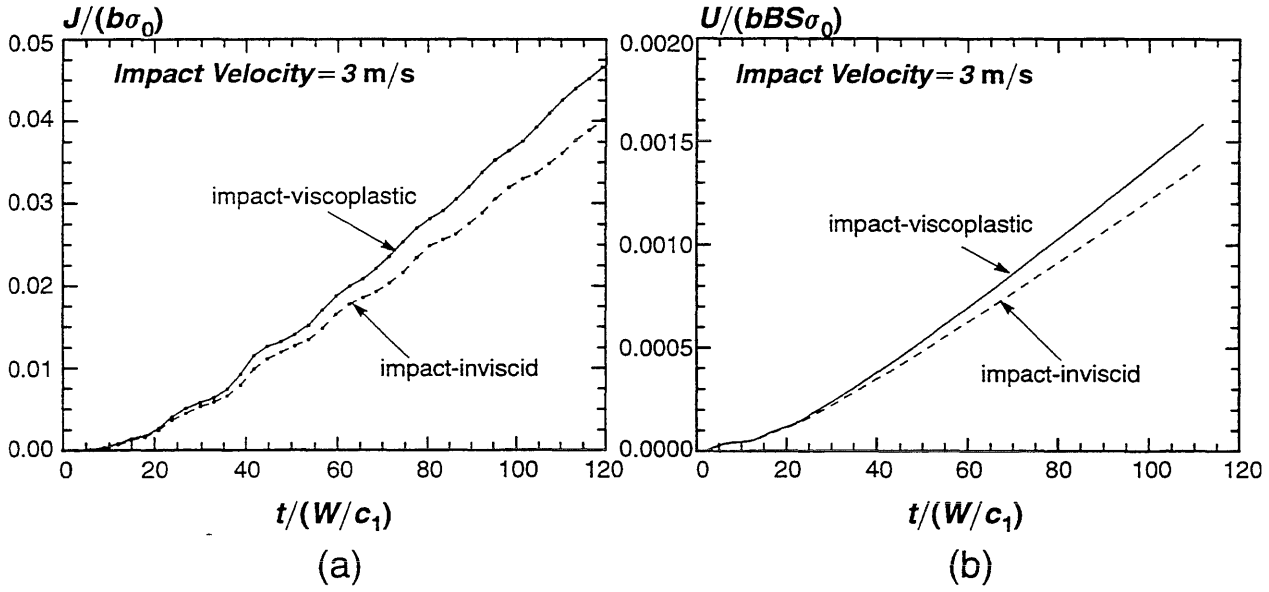

Figure 7. (a) Normalized applied–J as a function of normalized time; (b) Normalized internal energy as a function of normalized time. Where b is the uncracked ligament length, B the specimen thickness, S the specimen span and σ_0 the yield stress.

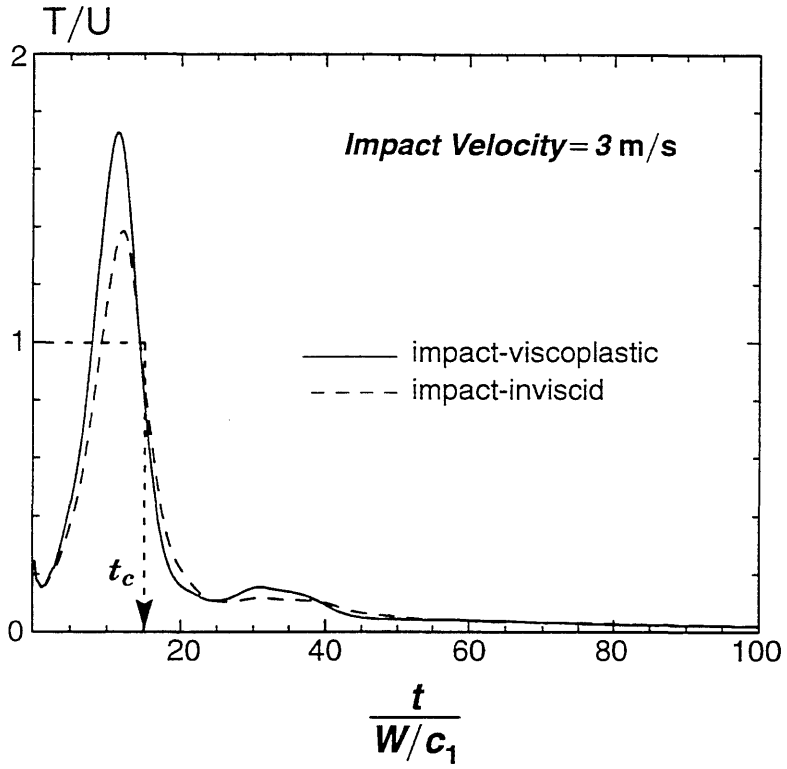

Figure 8. Energy ratios for impact loaded CVN specimen.

mura, et al. [16], extends beyond the support point by 0.1 W, where the CVN specimen extends beyond the support point by 0.75 W.

Table 1 lists transition times for the CVN specimen over a range of impact velocities. At velocities below 0.25 m/s, the energy ratio (T/U) remains significantly below unity for all time($t_c \approx 0$). The transition time increases with increasing impact velocity over the range 0.25 to 3 m/s. For the 6 m/s analysis, the energy ratio approaches, but never exceeds, unity (i.e. a transition time can no longer be defined). This observation suggests further examination of the internal and kinetic energies which constitute the energy ratio (see Figure 9). In the 6 m/s analysis, the internal energy increases more rapidly than the kinetic energy which yields an energy ratio less than unity for the entire specimen response. For the 3 m/s analysis, the internal energy increases *less* rapidly than the kinetic energy over the range $6 < t/(W/c_1) < 12$ which yields an energy ratio greater than unity over this time. The difference in energy response between the 3 and 6 m/s analyses indicates a limitation of the transition time based on a simple energy ratio. The original work of Nakamura, et al. [16] to develop the transition time assumes a specimen response approximated by simple beam bending. However, as the impact velocity increases, the deformation becomes more localized about the impact point, and the deformed shape of the specimen differs significantly from that of a beam in simple bending. The deformation in the 6 m/s analysis remains localized near the impact point early in the response; Figure10 shows the vertical displacements predicted by the 3 and 6 m/s analyses at $t \approx 14\,W/c_1$. The change in specimen response from a "bending" mode to a localized "punching" mode is apparent in this figure. The usefulness of the simple transition time concept appears limited to impact velocities < 6 m/s for pre-cracked CVN specimens. Another measure (e.g. the J–ratio discussed in the following section) may describe more accurately impact effects on crack-tip fields at high impact velocities.

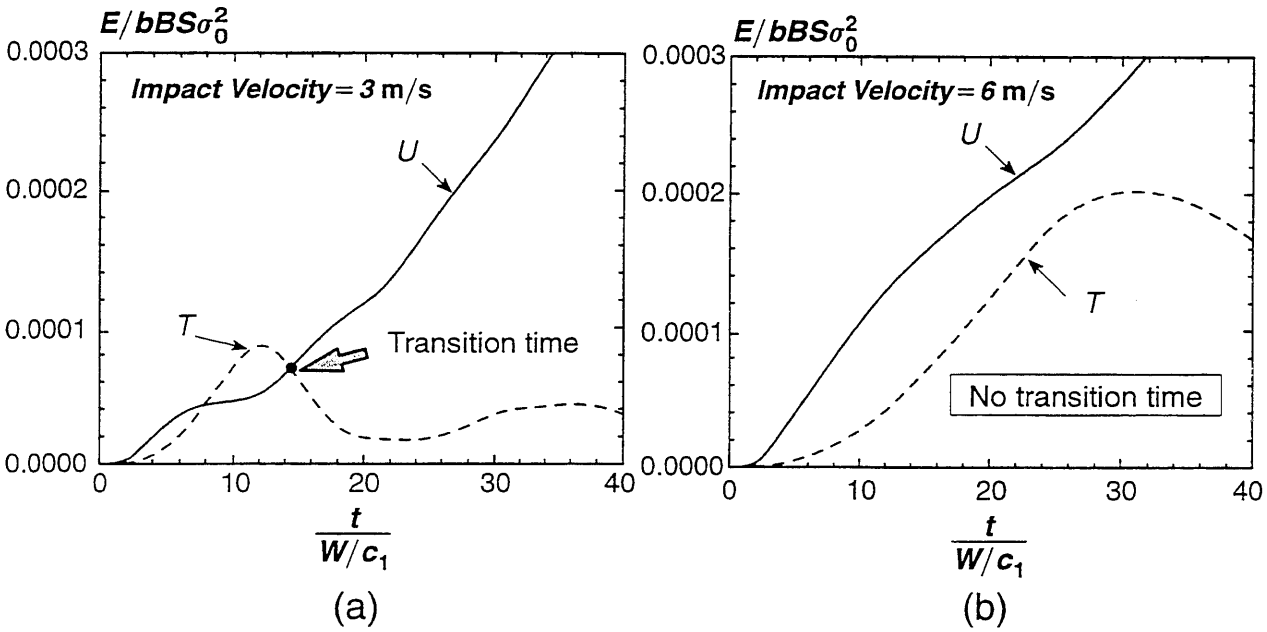

Figure 9. Normalized internal (U) and kinetic (T) energies as a function of normalized time for impact velocities of (a) 3 m/s and (b) 6 m/s.

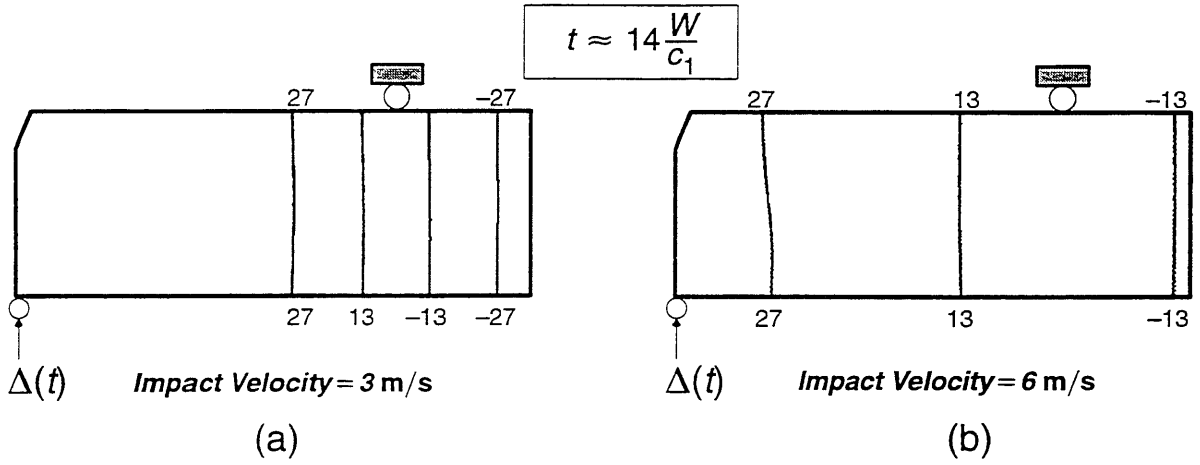

Figure 10. Contours of vertical displacement (v) at $t \approx 14\ W/c_1$ for impact velocities of (a) 3 m/s and (b) 6 m/s. The value of each contour is given in μm's adjacent to the contour.

Table 1: Effect of impact velocity on normalized transition time, $t_c\ /(c_1/W)$.

Impact Loading Rate (m/s)	From T/U	From J_{dyn}/J_{stat}
"Static"	≈ 0	≈ 0
0.025	≈ 0	≈ 0
0.25	1.5	≈ 0
1.0	5.5	≈ 0
3.0	14	13
6.0	≈ 0*	13

*Energy ratio (T/U) approaches, but never exceeds, unity

4.3 J-integral with Impact Loading Effects

For impact loading without crack extension, the "dynamic" J-integral formulation includes an additional term reflecting the kinetic energy density of material surrounding the crack tip [15]. The domain integral formulation adopted to calculate dynamic J–values in WARP3D includes this kinetic energy term; the volume integral for the kinetic energy term has the same form as the integral for strain energy density. WARP3D computes J-values, with and without this term, to quantify the relative importance of impact loading. Figure 11 shows the ratio of J–values including the kinetic energy term to conventional J–values neglecting this term. Deviations of the normalized J-values from unity, shown on the figure as a horizontal reference line, indicate the error incurred using the "static" formulation. At impact velocities below 3 m/s, the kinetic energy term has a negligible effect. As the impact velocity increases from 3 to 6 m/s, the kinetic energy term makes a strong contribution to the total J early in the response, lowering J substantially below the static value. However, for all loading rates considered, the static and dynamic J-values differ by less than 5% for $t \geq 13c_1/W$.

The ratio of J_{dyn} to J_{stat} offers a direct definition for the transition time independent of a specific deformation mode, e.g., beam bending, needed for the transition time based on the simple energy ratio. Once $J_{dyn}/J_{stat} \equiv 1$ inertial effects on J have vanished, and static formulas to compute experimental J-values from measured load and displacements apply. Table 1 compares the transition times computed from the J_{dyn}/J_{stat} ratio and transition times computed from the simple energy ratio. These transition times show excellent agreement for an impact velocity of 3 m/s; however, the transition times do *not* agree for either higher or lower impact velocities. The beam bending approach for development of the transition time employed by Nakamura, et al. [16] does not represent accurately the specimen response at other loading rates. Table 1 indicates that the energy ratio approach overestimates the transition time in CVN sized specimens for impact velocities < 3 m/s. At an impact velocity of 6 m/s, the energy ratio approach fails to provide an estimate of the transition time.

4.4 Load–Displacement Responses

Figure 12 shows the normalized force-time responses for the three CVN analyses. Both impact solutions exhibit similar early transients. The inviscid-impact solution agrees very well with the static solution for $t \geq 55W/c_1$ (typical times to brittle fracture are 90–120 W/c_1). The terminal region of the viscoplastic solution exhibits an elevation of 15% in the load compared to the inviscid and static solutions. This increase develops from elevation of the material yield strength throughout the plastic hinge region. Three specific times (39, 54, 101 W/c_1) are denoted by markers **A**, **B**, and **C**, respectively in Figure 12; reference is made to these times in the subsequent discussion to simplify correlations among different response quantities.

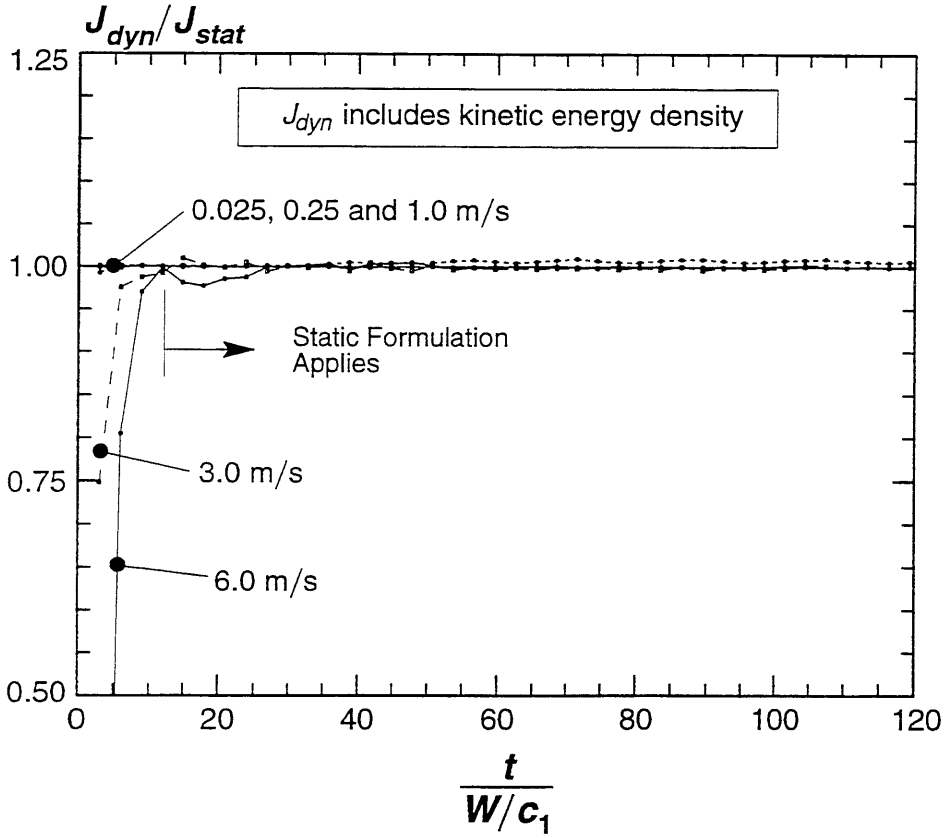

Figure 11. Ratio of dynamic J to static J as a function of normalized time for impact rates of 0.025, 0.25, 1.0, 3.0 and 6.0 m/s. Viscoplastic material response included in each analysis ($\eta = 1$, $m = 35$).

4.5 *J–Q* Trajectories

To examine the effects of impact loading on constraint in the CVN specimen, we adopt the J–Q and toughness scaling approaches described by O'Dowd and Shih [20], and Dodds, Shih and Anderson [8], respectively. The first methodology defines a continuum mechanics approach incorporating two parameters (J and Q) to characterize the near-tip stress field at the onset of fracture. Large-scale yielding in finite bodies causes a loss of the one-to-one correspondence between J and the near-tip fields. This loss of uniqueness, often termed *loss of constraint*, relaxes the near–tip stresses below their small–scale yielding values and produces an increase in fracture toughness. The continuum mechanics approach adopts a one-parameter family of self-similar solutions (Q–family) which describe the crack-tip fields under large-scale yielding. A simplified representation for the Q-family of fields within the forward sector ahead of the crack tip is

$$\sigma_{ij} = \left(\sigma_{ij}\right)_{\mathrm{SSY};T=0} + Q\sigma_0\delta_{1i}\delta_{1j} \tag{5}$$

where $(\sigma_{ij})_{\mathrm{SSY};T=0}$ denotes the infinite body stresses, σ_0 the yield strength, and δ_{ij} the Kronecker delta.

Operationally, Q is defined by

$$Q \equiv \frac{\sigma_{\theta\theta} - (\sigma_{\theta\theta})_{\mathrm{SSY;T=0}}}{\sigma_0}, \qquad \text{at } \theta = 0,\ r = 2J/\sigma_0 \tag{6}$$

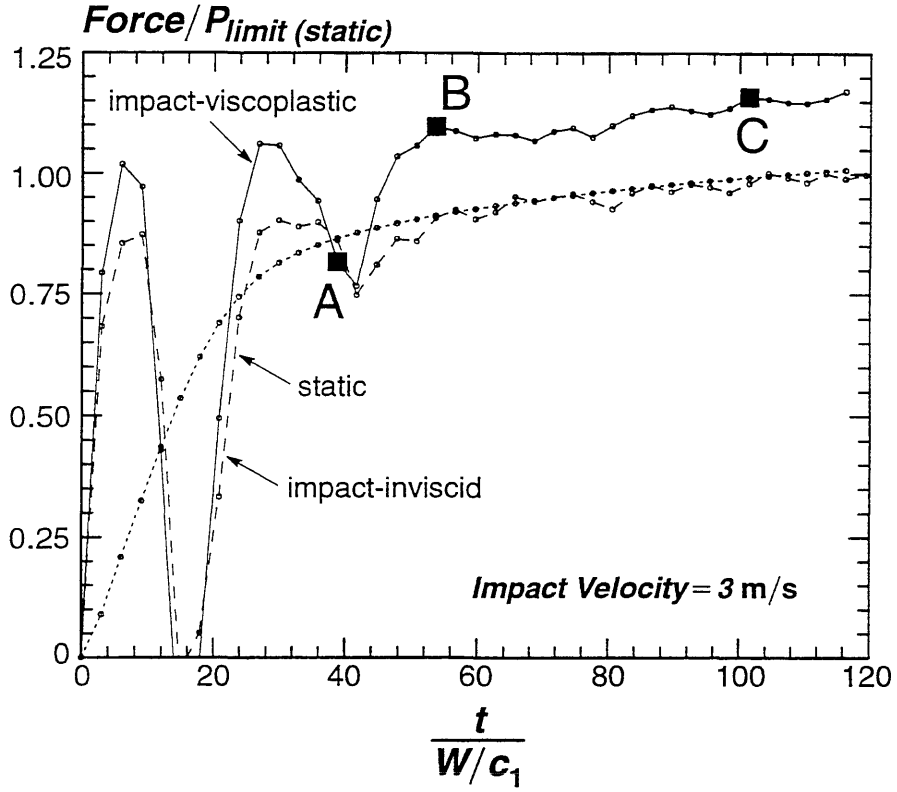

Figure 12. Normalized force versus time for three CVN analyses. $P_{limit\ (static)}$ denotes the computed static limit load for the CVN specimen. The discussion makes reference to the three times indicated by **A**, **B**, and **C**.

where the specimen stresses ($\sigma_{\theta\theta}$) in Eq (6) are evaluated from finite element analyses containing sufficient mesh refinement to resolve the fields at this length scale (where the fracture specimen and SSY model are loaded to the same J). No restrictions are imposed on the representation of material flow properties, e.g., Ramberg–Osgood. Large geometry changes may be included although values of Q derived from small geometry change analyses prove satisfactory in applications which make use of stresses outside the near–tip blunting region.

Figure 13 compares the J–Q trajectories for the static and two impact analyses. Q values are obtained from the finite element solutions of opening-mode stresses on the crackplane using the operational definition given in Eq. (6). The loading rate applied to the $SSY_{T=0}$ reference analysis, $\dot{K}_I = 11\ GPa\sqrt{m}\ /s$, approximates the crack-tip loading rate calculated from the CVN analysis for an impact velocity of 3 m/s. A positive value of Q indicates that the crack-tip stresses exceed the values for $SSY_{T=0}$ (a high triaxiality condition); whereas a negative value of Q signals a loss of constraint. An initial transient in the impact-inviscid solution dissipates by $t = 30\,W/c_1$. For $t > 30\,W/c_1$, the J–Q trajectory for the impact-inviscid solution shows close agreement with the static solution. The viscoplastic solution produces initially large, positive Q–values which decrease rapidly with time (and increasing load), becoming negative at approximately $t = 55\,W/c_1$. After this time, the viscoplastic J–Q trajectory slowly approaches the static response.

The impact force *vs.* time response of this analysis shows that t must exceed $55\,W/c_1$ for close agreement with the static solution. The effects of impact loading on the specimen thus dissipate more quickly in the crack–tip region than globally. Impact testing of precracked bend specimens, conducted previously by Böhme [6], verifies this phenomenon experimentally. In

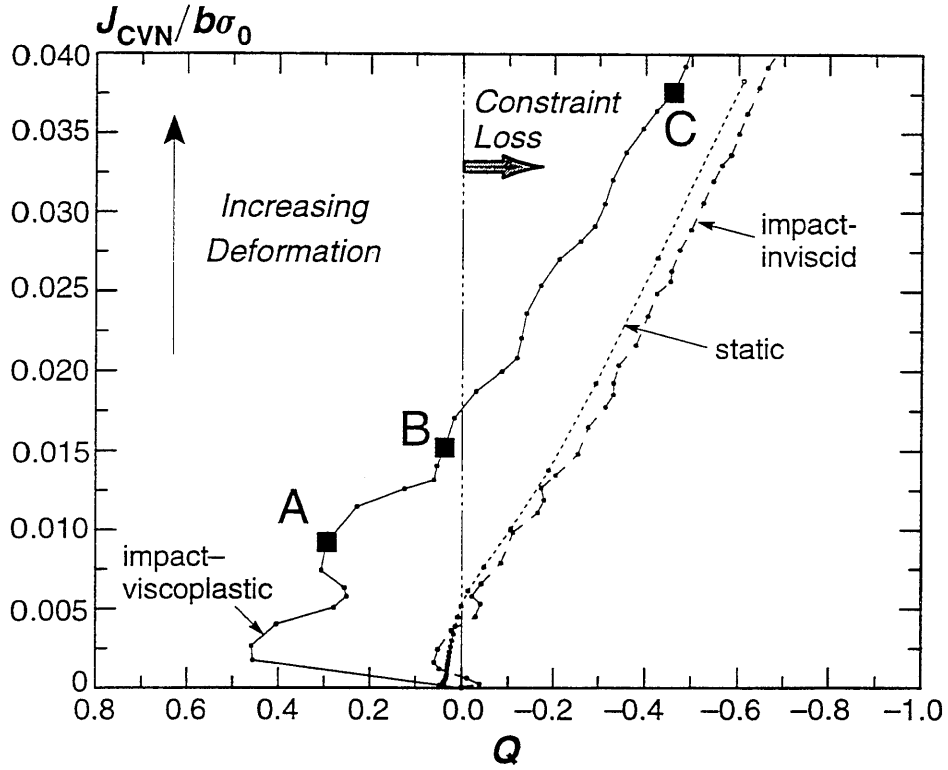

Figure 13. *J-Q* trajectories for static, impact-inviscid, and impact-viscoplastic solutions (impact velocity = 3 m/s).

his work, Böhme measured K_I^{dyn} through the method of caustics and determined the time at which K_I^{dyn} begins to agree closely with the quasi-static formulation. Through a comparison of his results with those of Ireland [11] and Nakamura, et al. [16], Böhme concluded the effects of impact loading diminish at the crack-tip earlier than in the measured loads.

Table 2: Effect of impact loading rate on deformation limits to maintain SSY conditions as developed from *J–Q* trajectories ($M_{J\text{-}Q}$) and toughness scaling model (M_{TSM}).

Impact Loading Rate (m/s)	$M_{J\text{-}Q}$	M_{TSM}
"Static"	200	200
0.025	150	190
0.25	100	120
1.0	75	90
3.0	60	70
6.0	60	70

The impact-viscoplastic solution indicates that the deformation level at constraint loss, where Q changes from positive-to-negative, exceeds that for the static solution by a factor of approximately three. Such specimen size and deformation limits to maintain SSY conditions are commonly expressed in the form $min(a,b) > MJ/\sigma_0$ where M for the static solution in Fig. 13 takes on the value 200 and for the viscoplastic solution $M = 60$. Table 2 lists the values of M over a range of loading rates. The slowest impact loading rate considered (0.025 m/s) ele-

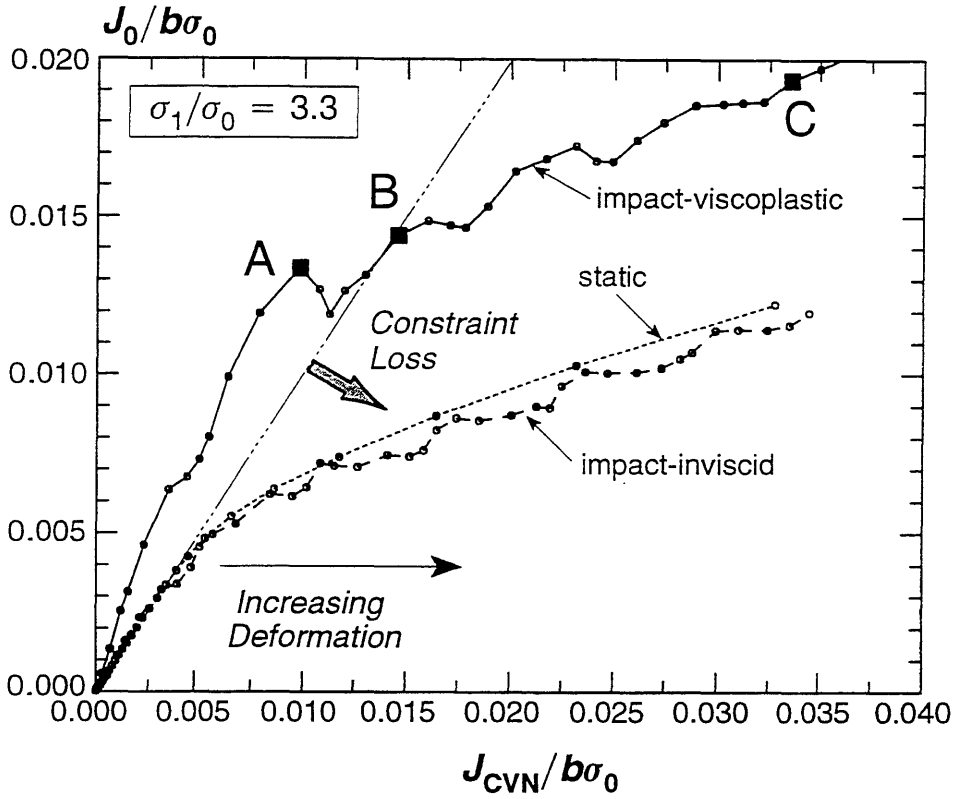

Figure 14. Comparison of J in CVN specimen (J_{CVN}) and J_0 for analyses including different features (impact velocity = 3 m/s). These trajectories are developed from a principal stress ratio of $\sigma_1/\sigma_0 = 3.3$.

vates the deformation limit by 25% compared to the static loading. The deformation limit increases with increasing loading rate for impact velocities below 3 m/s. For impact velocities between 3 and 6 m/s, the deformation limit (M value) remains constant.

4.6 Toughness Scaling Model

The toughness scaling methodology quantifies the effect of constraint loss on the non-linear relationship between the micro-scale crack driving force (e.g. near-tip stresses) and macro-scale crack driving force (e.g. J, CTOD). This methodology does not attempt to predict J_c–values from metallurgical parameters; rather it predicts the variation of cleavage fracture toughness with constraint changes by scaling to the $SSY_{T=0}$ condition as a convenient reference. For steels operating in a temperature range over which cleavage occurs after significant plastic deformation, but before the initiation of ductile growth (lower to mid-transition), the volume of material within principal stress contours enclosing the crack–tip defines a realistic local failure criterion for use in this approach [22] . Specimens with the same stressed volumes of material are considered to have the same probability for cleavage fracture, even though the J–values may differ significantly due to large-scale yielding effects.

Figure 14 shows the effects of impact loading in terms of the toughness scaling model. Points on the response curves correspond to equal probability of cleavage fracture, i.e. equal stressed volumes of material within specified principal stress contours. J_0 denotes the J-value needed under $SSY_{T=0}$ conditions to achieve the same stressed volume as in the precracked CVN specimen when loaded to J_{CVN}. A line of unit slope indicates the $SSY_{T=0}$ condition; when a loss of constraint relative to this condition occurs, the CVN solution falls below this line. A

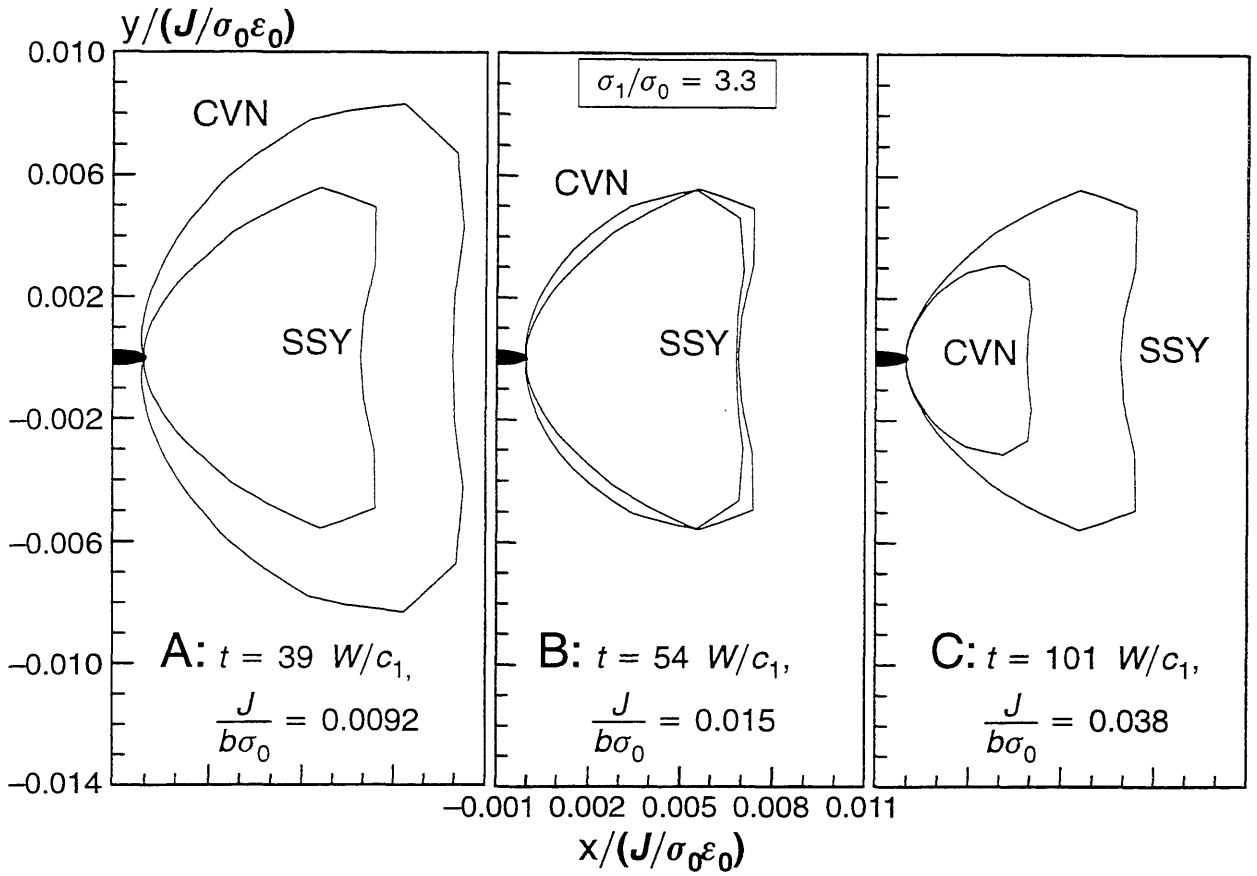

Figure 15. Normalized principal stress contours at three times following impact.

small initial transient in the impact-inviscid solution diminishes rapidly and this solution merges with the static solution. In contrast, the impact-viscoplastic solution shows a significant elevation in constraint. The toughness scaling model also indicates an increase in the deformation level (M) at which a loss of constraint occurs of approximately three over the static solution. Table 2 also gives the deformation limits developed from the toughness scaling model. For each of the rates considered, the toughness scaling model predicts a slightly smaller M-value at constraint loss compared to the J–Q model. The deformation limit determined from the toughness scaling model indicates an increase of only 5% for the slowest impact velocity considered (0.025 m/s). Both the J-Q and the toughness scaling models predict a constant deformation limit over impact velocities of 3 and 6 m/s.

Figure 15 compares the principal stress contour ($\sigma_1/\sigma_0 = 3.3$) for the impact-viscoplastic analysis with the $SSY_{T=0}$ model at the three reference points **A**, **B**, **C**. With normalization of material point positions from the tip (x, y) by $J/\sigma_0\varepsilon_0$, the $SSY_{T=0}$ contours remain invariant for all J. At reference point **A** during the response of the CVN specimen, the impact-viscoplastic contour encloses a significantly larger area compared to $SSY_{T=0}$ solution. As deformation in the CVN increases and a constraint loss occurs, the area within the principal stress contour increases but at a rate slower than for the $SSY_{T=0}$ solution. Consequently, the normalized size of the CVN contour decreases. The CVN and $SSY_{T=0}$ contours appear approximately identical at reference point **B**, and once the deformation history reaches reference point **C**, the CVN contour shows a significant loss of constraint relative to $SSY_{T=0}$.

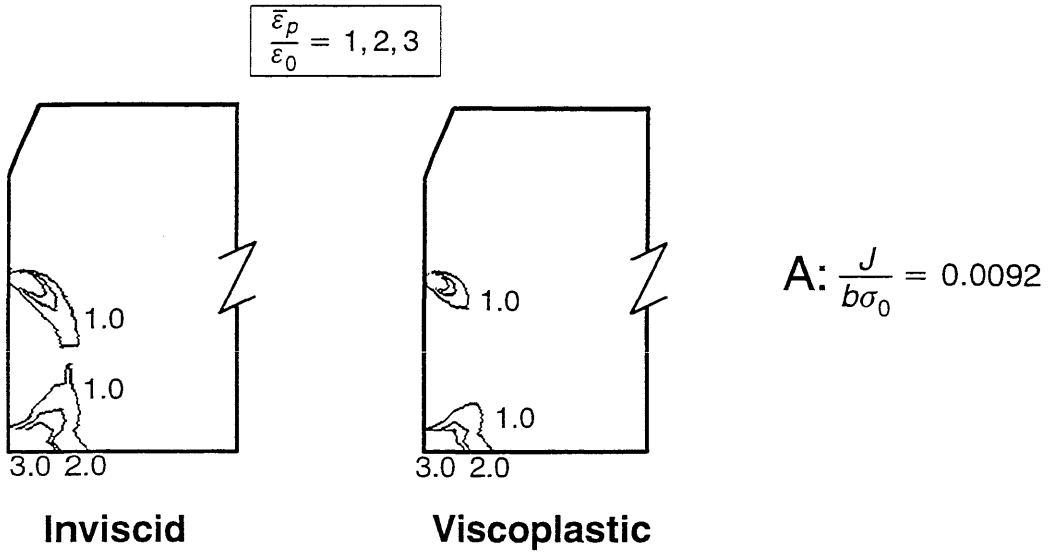

Figure 16. Fringes of equivalent plastic strain normalized by the static yield strain (ε_0). The label **A** refers to a point during the viscoplastic response. The viscoplastic and inviscid models are compared at the same value of J. Impact velocity is 3 m/s.

Because the $SSY_{T=0}$ model includes viscoplastic effects in the reference state ($\dot{K}_I = 11\ GPa\sqrt{m}/s$), the large difference between the principal stress contours early in the loading must arise from viscoplastic effects in the CVN specimen away from the crack-tip. The nearly identical solutions for the inviscid-impact and static analyses eliminate inertia as a contributing factor. The impact bending load creates a large gradient in strain rates across the remaining ligament of the specimen which elevates the yield stress sufficiently to maintain SSY conditions to much higher J–levels. To assess the effect of this strain gradient on plastic flow, fringes of equivalent plastic strain ($\bar{\varepsilon}_p$) are shown in Figure 16 for a reference point during the response (**A**). The viscoplastic solution at **A** reveals a crack-tip plastic zone contained within an elastic field; whereas, the crack-tip plastic zone for the inviscid solution connects with the plastic zone from the impact point. The elevated strain rates from impact loading increase the yield strength and inhibit plastic flow across the entire ligament in the viscoplastic solution sufficient to maintain SSY conditions.

The differences in plastic strain contours for the inviscid and viscoplastic solutions diminish with increasing time and deformation. The inviscid and viscoplastic solutions both show significant plastic flow across the entire ligament at **B**. Once the deformation increases to **C**, the plastic zones appear approximately equal although stresses within the near-tip zone of the viscoplastic solution remain higher due to the continued yield stress elevation.

4.7 Material Rate Sensitivity Effects on M

We performed a parametric study to quantify the effect of viscoplastic material response (as specified by η in Eq. 4) on the size/deformation limit factor, M. Figure 17 shows the spatial variation of equivalent strain rate ($\dot{\bar{\varepsilon}}$) for a viscoplastic analysis performed at an impact rate of 3 m/s using properties of a moderately rate sensitive material ($\eta = 10^3$). The non-yielded material within the remaining ligament experiences $\dot{\bar{\varepsilon}} \approx 1000$. The suppression of yielding within this region constrains the plastic flow, and the precracked CVN remains under SSY conditions to higher deformation levels than the rate insensitive analyses. We chose $\dot{\varepsilon} = 1000$ as the reference strain rate to determine the effect of varying η on the material model defined by Eq. 4. Figure 18 shows four uniaxial stress-strain curves (parametric in η) developed from this visco-

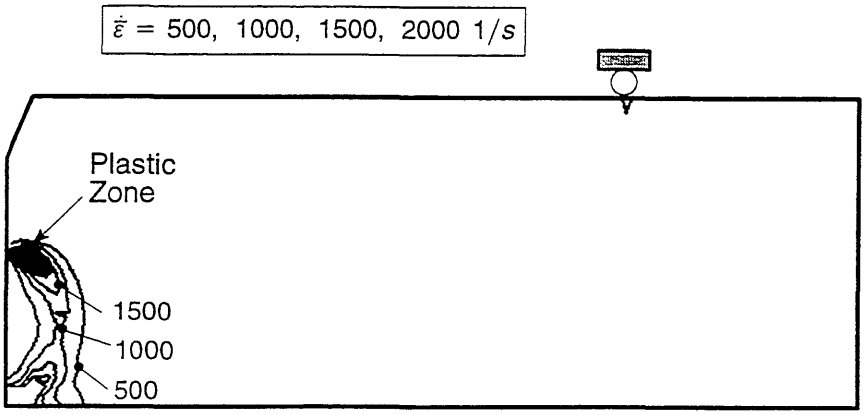

Figure 17. Contours of equivalent strain rate in precracked CVN specimen for an impact velocity of 3 m/s ($m = 35$, $\eta = 10^3$). These results are typical of all 3 m/s analysis prior to Large Scale Yielding. The plastic zone is indicated by the solid region at the crack tip.

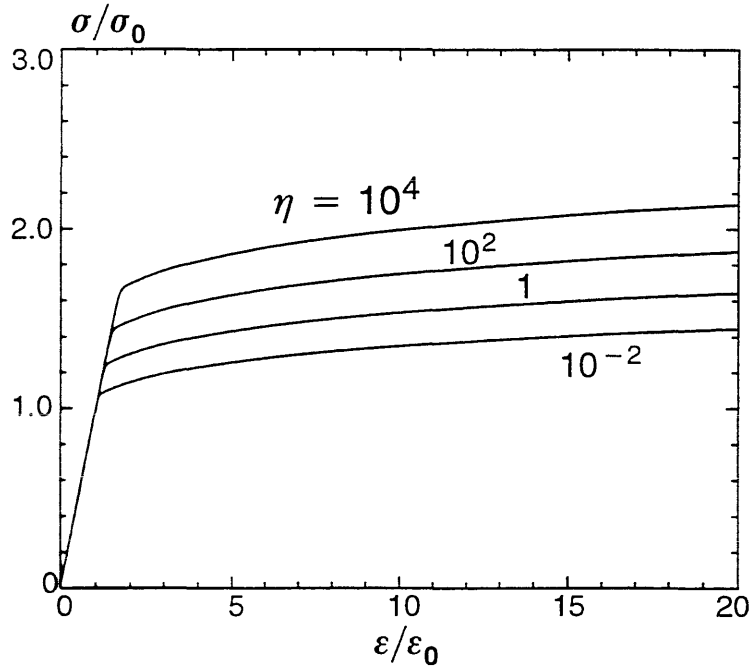

Figure 18. Normalized stress-strain curves over a range of η values (strain rate = 10^3 1/s, $m = 35$ for each curve).

plastic model at $\dot{\varepsilon} = 1000$. The four η values characterize materials exhibiting low ($\eta = 10^{-2}$), moderate ($\eta = 1 \rightarrow 1000$), and high ($\eta = 10^4$) strain rate sensitivity.

All of these analyses were conducted at an impact rate of 3 m/s which represents the lower-limit of impact rates specified by ASTM E–23. Figure 19 shows the effect of varying η on the limit load. The limit load increases by 3, 15, 30 and 45 percent for analyses with $\eta = 10^{-2}$, 1, 10^2 and 10^4, respectively.

Figure 20 shows that M varies between the static limit (200) and 25–30 for a strongly rate sensitive material. The M values developed from the J-Q and TSM approaches show good agreement over a large range of material rate sensitivity.

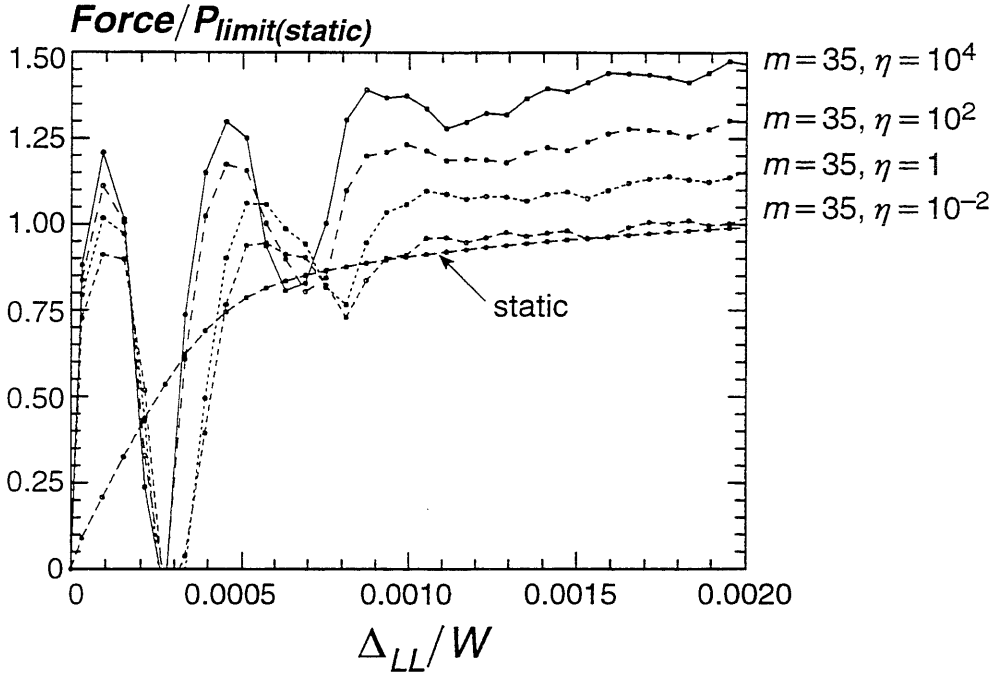

Figure 19. Force versus loadline displacement for a range of viscoplastic material responses.

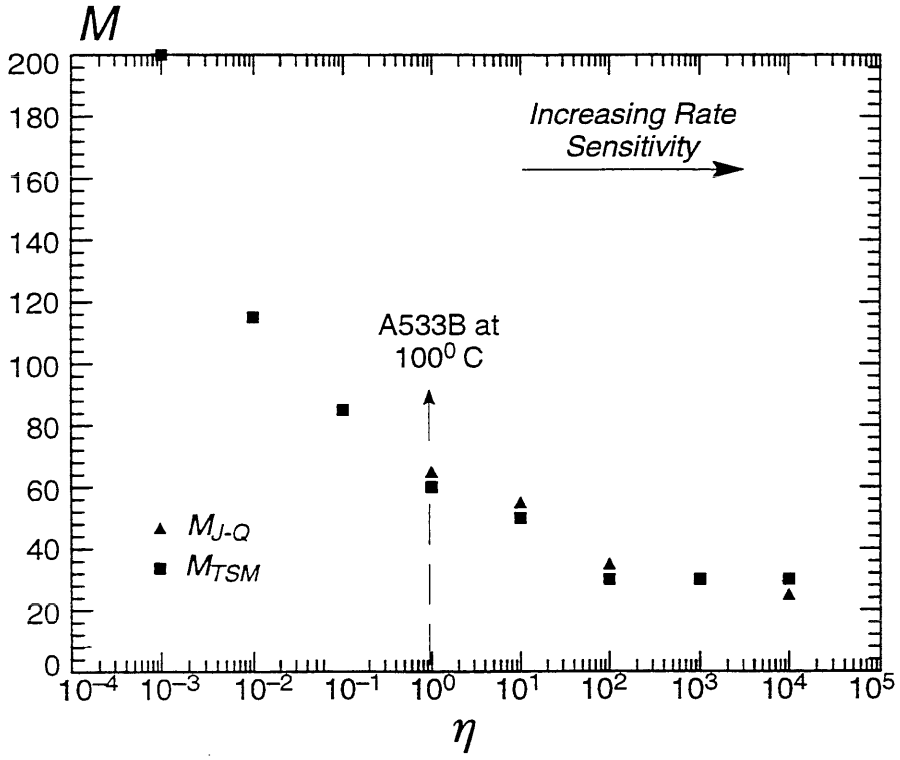

Figure 20. Effect of material strain-rate sensitivity on deformation limits to maintain SSY conditions as developed from J–Q trajectories ($M_{J\text{-}Q}$) and toughness scaling model (M_{TSM}).

5. Discussion

The combination of specimen size and material flow properties limits the maximum J_c -values that can be measured under conditions of SSY in pre-cracked CVN specimens loaded statically or by impact. Measured J_c -values greater than the SSY limits should be corrected for the loss of constraint. Unfortunately, the fracture toughness of most structural steels exceeds the SSY deformation limit for static loading on CVN specimen sizes. Consider a material having a yield strength $\sigma_0 = 450$ MPa, E = 206,850 MPa, $b = 5$ mm; then maximum static J before constraint loss (using M from Table 2) is 11.3 kJ/m^2 ($K_{Jc} = 50$ MPa$\sqrt{m}$). However, analysis results presented here demonstrate that even "slow" impact testing of moderately rate-sensitive materials elevates significantly the deformation limit at constraint loss. The impact-viscoplastic analysis indicates an increase of the (J) deformation limit by a factor of approximately 2.2 for an impact velocity of 1 m/s and an increase of 3.0 for an impact velocity of 3 m/s for a material with hardening exponent $n = 10$ and moderate rate sensitivity. Consider again the material with static yield stress of $\sigma_0 = 450$ MPa, the maximum impact J before constraint loss (using M from Table 2 for 3 m/s impact velocity) is 32 kJ/m^2 ($K_{Jc} = 85$ MPa$\sqrt{m}$). Current work does not address the relationship between such impact J_c values and conventional, static values. The J_c-values measured during impact tests appear applicable only in assessments of structural flaws which experience loading rates similar to those imposed in the impact toughness tests.

We emphasize again the 2-D (plane-strain) nature of the present impact analyses. Recently completed 3-D analyses of conventional deep notch SE(B) specimens subjected to static loading demonstrate substantially larger J-values at loss of SSY yielding conditions (M values of 50–100 rather than the plane-strain value of 200) [17]. Similar 3-D analyses for impact loading may indicate a further relaxation of M values into the 25–50 range for moderately rate-sensitive materials. Such M values would increase the maximum J_c-values measurable under SSY conditions in a CVN specimen for the example material above to 90 kJ/m^2 ($K_{Jc} = 145$ MPa$\sqrt{m}$).

References

[1] Anderson, T.L. and Dodds, R.H., Jr., "Specimen Size Requirements for Fracture Toughness Testing in the Transition Region," *Journal of Testing and Evaluation*, JTEVA, Vol. 19, No. 2, March 1991, pp.123–134.

[2] ASTM E23–91, "Standard Test Methods for Notched Bar Impact Testing of Metallic Materials," American Society for Testing and Materials, Philadelphia, (1991).

[3] ASTM E1152–87, "Standard Test Methods for Notched Bar Impact Testing of Metallic Materials," American Society for Testing and Materials, Philadelphia, (1991).

[4] Ayers, D. J., "Dynamic Plastic Analysis of Ductile Fracture – the Charpy Specimen," *International Journal of Fracture*, Vol. 12, pp. 567–578, (1976).

[5] Barsom, J. M. and Rolfe, S. T., "Correlations Between K_{Ic} and Charpy V-Notch Test Results in the Transition-Temperature Range," *Impact Testing Of Metals, ASTM STP 466,* American Society for Testing and Materials, Philadelphia, pp. 281–302, (1970).

[6] Böhme, W., "Dynamic Key-Curves for Brittle Fracture Impact Tests and Establishment of a Transition Time," *Fracture Mechanics: Twenty-First Symposium, ASTM STP 1074*, J.P. Gudas, J.A. Joyce, and E.M. Hackett, Eds., AMerican Society for Testing and Materials, Philadelphia, pp. 144–156, (1990).

[7] Böhme, W., and Kalthoff, J.F. "The Behavior of Notched Bend Specimens in Impact Testing," *International Journal of Fracture*, Vol. 20, pp. R139–R143, (1982).

[8] Dodds, R.H., Jr., Shih, C.F., Anderson, T.L., "Continuum and Micromechanics Treatment of Constraint in Fracture," *International Journal of Fracture,* Vol. 64, pp. 101–133, (1993).

[9] Gurson, A.L., "Continuum Theory of Ductile Rupture by Void Nucleation and Growth: Part I–Yield Criteria and Flow Rules for Porous Ductile Media," *Journal of Engineering Materials and Technology,* Vol. 99, pp. 2–15, (1977).

[10] Hughes, T.J. "Generalization of Selective Integration Procedures to Anisotropic and Nonlinear Media," *International Journal for Numerical Methods in Engineering*, Vol. 15, pp 1413–1418, (1980).

[11] Ireland, D.R., "Critical Review of Instrumented Impact Testing," *Proceedings of the International Conference on Dynamic Fracture Toughness,* London, pp. 47–62, (1976).

[12] Koppenhoefer, K. C., Gullerud, A. S., Ruggieri, C., and Dodds, R. H., Jr. "WARP3D: Dynamic Nonlinear Analysis of Solids Using a Preconditioned Conjugate Gradient Software Architecture," *Civil Engineering Studies,* SRS No. 596, UILU–ENG–94–2017, University of Illinois, Urbana, Illinois, (1994).

[13] Marandet, B. and Sanz, G., "Evaluation of the Toughness of Thick Medium-Strength Steels by Using Linear-Elastic Fracture Mechanics and Correlations Between K_{Ic} and Charpy V–Notch,", *ASTM STP 631,* American Society for Testing and Materials, Philidelphia, pp. 72–95, (1977).

[14] McMeeking, R.M., "Finite Deformation Analysis of Crack-Tip Opening in Elastic-Plastic Materials and Implications for Fracture," *Journal of the Mechanics and Physics of Solids*, Vol. 25, pp. 357–381, (1977).

[15] Nakamura, T., Shih, C. F., and Fruend, L. B., "Elastic-Plastic Analysis of a Dynamically Loaded Circumferentially Notched Round Bar," *Engineering Fracture Mechanics*, Vol. 22, pp. 437–452, (1985).

[16] Nakamura, T., Shih, C. F., and Fruend, L. B., "Analysis of a Dynamically Loaded Three-Point-Bend Ductile Fracture Specimen," *Engineering Fracture Mechanics*, Vol. 25, pp. 323–339, (1986).

[17] Nevalainen, M., and Dodds, R.H., Jr., "Numerical Investigation of 3-D Constraint Effects on Brittle Fracture in SE(B) and C(T) Specimens," *Submitted to International Journal of Fracture.*

[18] Newmark, N.M., "A Method of Computation for Structural Dynamics," *Journal of the Engineering Mechanics Division*, ASCE, Vol. 32, No. EM3, pp 67–94, (1959).

[19] Norris, D. M., Jr., "Computer Simulation of the Charpy V–Notch Toughness Test," *Engineering Fracture Mechanics,* Vol. 11, pp. 261–274, (1979).

[20] O'Dowd, N.P., and Shih, C.F., "Family of Crack-Tip Fields Characterized by a Triaxiality Parameter–I. Structure of Fields," *Journal of Mechanics and Physics of Solids*, Vol. 39, No. 8, pp. 989–1015, (1991).

[21] Rice, J.R., and Tracey, D.M., in *Numerical and Computer Methods in Structural Mechanics,* S.J. Fenves, et al. (eds.), Academic Press, New York, pp. 585–623, (1968).

[22] Ritchie, R. O., Knott, J.F., and Rice, J.R., "On the Relationship Between Critical Tensile Stress and Fracture Toughness in Mild Steel," *Journal of the Mechanics and Physics of Solids,* Vol. 21, pp. 395–410, (1973).

[23] Ritchie, R. O. "On the Relationship Between Fracture Toughness and Charpy V–Notch Energy in Ultrahigh Strength Steel," *What Does The Charpy Test Tell Us?*, American Society for Metals, pp. 54–73, (1978).

[24] Sailors, R. H. and Corten, H. T., "Relationship between Material Fracture Toughness using Fracture Mechanics and Transition Temperature Tests," *Fracture Toughness, Proceedings of the 1971 National Symposium on Fracture Mechanics, Part II, ASTM STP 514,* American Society for Testing and Materials, pp. 164–191, (1972).